Septins regulate junctional integrity of endothelial monolayers

Joanna Kim and John A. Cooper*

Departments of Biochemistry & Molecular Biophysics and Cell Biology & Physiology, Washington University, St. Louis, MO 63110

ABSTRACT Junctional integrity of endothelial monolayers is crucial to control movement of molecules and cells across the endothelium. Examining the structure and dynamics of cell junctions in endothelial monolayers, we discovered a role for septins. Contacts between adjacent endothelial cells were dynamic, with protrusions extending above or below neighboring cells. Vascular endothelial cadherin (VE-cadherin) was present at cell junctions, with a membrane-associated layer of F-actin. Septins localized at cell-junction membranes, in patterns distinct from VE-cadherin and F-actin. Septins assumed curved and scallop-shaped patterns at junctions, especially in regions of positive membrane curvature associated with actin-rich membrane protrusions. Depletion of septins led to disrupted morphology of VE-cadherin junctions and increased expression of VE-cadherin. In videos, septin-depleted cells displayed remodeling at cell junctions; regions with VE-cadherin were broader, and areas with membrane ruffling were wider. Septin depletion and junction disruption led to functional loss of junctional integrity, revealed by decreased transendothelial electric resistance and increased transmigration of immune cells. We conclude that septins, as cytoskeletal elements associated with the plasma membrane, are important for cell junctions and junctional integrity of endothelial monolayers, functioning at regions of positive curvature in support of actin-rich protrusions to promote cadherin-based cell junctions.

INTRODUCTION

The endothelial monolayer is a continuous thin layer of endothelial cells that lines the interior surface of blood and lymphatic vessels. The endothelium is the interface between the blood or lymph and the interstitial tissue spaces, and the endothelial monolayer functions as an active and regulated barrier (Baldwin and Thurston,

2001). The endothelial barrier plays crucial roles in multiple biological processes, including vascular tone, thrombosis/thrombolysis, cell adhesion, and passage of small molecules and cells. To perform these diverse roles, maintenance and regulation of the barrier structure and monolayer integrity are crucial (Sumpio *et al.*, 2002; Michiels, 2003; Deanfield *et al.*, 2007). In some settings, such as liver sinusoids, the barrier is quite permeable, with spaces called fenestrae between the endothelial cells (Lalor *et al.*, 2006; Poisson *et al.*, 2017). In other settings, notably the brain, the barrier is relatively tight, and endothelial cells form a robust monolayer with strong cell–cell junctions. In the setting of inflammation, the integrity of the monolayer can be regulated to allow cells and molecules to move between the blood and the interstitial space (Pachter *et al.*, 2003; Abbott *et al.*, 2006).

The integrity of the endothelial monolayer depends on endothelial cell–cell junctions, which include adherens junctions and tight junctions (Bazzoni and Dejana, 2004; Dejana, 2004; Lampugnani *et al.*, 2017). Vascular endothelial cadherin (VE-cadherin) is a prominent adhesive component of endothelial adherens junctions, and endothelial tight junctions include adhesion molecules such as ZO-1, claudins, occludin, junctional adhesion molecules, and the

nectin–afadin system. The cell junctions are supported in the cytoplasm by elements of the cytoskeleton associated with the plasma membrane, notably actin filaments (F-actin) (Hartsock and Nelson, 2008).

The actin cytoskeleton and its regulatory proteins play important roles in the function of endothelial cell monolayers; they control the assembly and stability of cell–cell junctions (Mooren *et al.*, 2014, 2015; Schnittler *et al.*, 2014; Garcia-Ponce *et al.*, 2015). The formation of VE-cadherin–based cell junctions between endothelial cells is promoted by actin-based lamellipodia termed "junction-associated intermittent lamellipodia" (Abu Taha *et al.*, 2014), including during angiogenesis (Cao *et al.*, 2017). Branched actin networks appear to push membranes of adjacent cells toward each other to promote VE-cadherin interactions (Efimova and Svitkina, 2018).

Septins are another important element of the membrane-associated cytoskeleton (Spiliotis and Gladfelter, 2012; Bridges and Gladfelter, 2015; Valadares *et al.*, 2017). Septin family proteins form homo- and hetero-oligomers in vitro and in vivo (Bridges and Gladfelter, 2015; Valadares *et al.*, 2017), and those oligomers associate directly with lipid membranes and assemble into filaments (Bridges *et al.*, 2014). The membrane-associated filaments form ring- and gauze-shaped higher-order arrays in cells and in vitro (Rodal *et al.*, 2005; Ong *et al.*, 2014; Bertin *et al.*, 2012). Filaments form preferentially in areas of positive membrane curvature (Bridges and Gladfelter, 2015; Bridges *et al.*, 2016; Kang and Lew, 2017), providing interactive feedback between cell shape and the cytoskeleton.

Discovered as important for cell division in budding yeast (Haarer and Pringle, 1987; Ong *et al.*, 2014), septins are distributed widely across different types of eukaryotic cells. Their diverse functions in mammalian systems, which include mitochondrial fission (Pagliuso *et al.*, 2016) and endomembrane fusion (Dolat and Spiliotis, 2016), have been active areas of study (Spiliotis and Nelson, 2006; Dolat *et al.*, 2014; Fung *et al.*, 2014). Septins interact with elements of the actin and microtubule cytoskeleton to control and coordinate cell shape and movement in a variety of cell settings (Joo *et al.*, 2007; Spiliotis *et al.*, 2008; Spiliotis, 2018; Hu *et al.*, 2012; Mavrakis *et al.*, 2014; Bezanilla *et al.*, 2015).

Our ongoing studies of transendothelial migration led us to investigate the roles for septins at endothelial cell–cell junctions. In earlier work, we found that actin assembly, controlled by regulators of Arp2/3 complex, was important for the assembly and dynamics of endothelial cell junctions (Mooren *et al.*, 2014, 2015). Here we investigated potential roles for septins in endothelial monolayers. We report that septins associate with regions of the plasma membrane with positive curvature and that septins are important for proper assembly of VE-cadherin–based junctions and for the barrier function of the endothelial monolayer.

RESULTS

Cell–cell junctions of the endothelial monolayer: surface views

To understand how septins might contribute to endothelial cell–cell junctions and the integrity of endothelial monolayers, we began by examining the morphology of cell junctions in a cell culture system—monolayers of primary human dermal microvascular endothelial cells (HDMVECs). Examining the dorsal surface of HDMVEC monolayers with surface scanning electron microscopy, we found the cells to be large and flat, forming a continuous monolayer (Figure 1). Boundaries between cells in the monolayer were predominantly straight and smooth, extending over appreciable distances. In a number of places, membrane ruffles were observed

at cell edges; and in other places, protrusions were observed, with one cell extending over the top of a neighboring cell.

Septins at endothelial cell borders: positive curvature

To investigate potential roles for septins as elements of the membrane cytoskeleton in endothelial monolayers, we localized septin 2 in our preparations. We performed multicolor imaging of HDMVEC monolayers stained with antibodies against septin 2 and VE-cadherin, along with fluorescent phalloidin to visualize F-actin. Septin 2 was found near cell–cell junctions, as defined by the presence of VE-cadherin. High-magnification views revealed that septin 2 did not colocalize completely and precisely with VE-cadherin or with F-actin (Figure 2); distinct differences were apparent. Similar results were obtained for endothelial monolayers derived from primary microvascular endothelial cells derived from human brain (Supplemental Figure 1).

To understand the organization of septin 2 in more detail, we examined the fluorescent stained samples with superresolution microscopy, using a structured illumination system (Nikon N-SIM). Septin 2 appeared in curved and scallop-shaped structures at the junctions, in the region of VE-cadherin and F-actin (Figure 3). The presence of these curved structures was confirmed by scanning confocal microscopy (Nikon A1R; Supplemental Figure 2). Septins are known to interact directly with lipid membranes with positive curvature (Bridges *et al.*, 2016).

In these samples, stained for endogenous septin 2, one cannot determine whether the membrane curvature is positive or negative because the images visualized endogenous septin 2 from adjacent cells. To determine which cell showed curved septin 2 staining and whether the curvature was negative or positive, we expressed septin 2 tagged with a fluorescent protein. Sets of HDMVECs were infected with lentivirus expressing either septin 2-GFP or septin 2-td-Tomato separately, and the cells were combined and cocultured with each other and with uninfected cells. At boundaries of septin 2-GFP cells with septin 2-tdTomato cells, and at boundaries of fluorescent cells with nonfluorescent cells, the images revealed that membrane-associated septin 2 was associated with regions of positive curvature in the plasma membrane of the cell expressing the tagged septin 2 (Figure 4). The images revealed more curved septin 2 formations in regions where cell protrusions were present, relative to regions at rest, suggesting that septin 2 assembly and membrane protrusion are in concert.

To look for association of septin 2 with regions of membrane protrusion, we coinfected cells with lentivirus expressing septin 2-tdTomato and VE-cadherin-GFP. VE-cadherin-GFP served as a general marker for the plasma membrane, because VE-cadherin is distributed continuously over the entire plasma membrane, in addition to its prominent accumulation at cell junctions. These cells were mixed with uninfected cells to form a monolayer. Septin 2-tdTomato was concentrated in curved structures near the base and along the sides of membrane protrusions (Figure 5). At nonprotruding resting regions of membranes, fluorescent septin 2 was present as linear elements associated with the membrane, but it was not concentrated in those regions (Figure 5).

Analysis of associated septins

Septin family members assemble into heteromeric oligomers and filaments in vitro and in vivo (Finnigan *et al.*, 2016; Valadares *et al.*, 2017). We investigated whether other septin family members were associated with septin 2 at cell junctions in HDMVEC monolayers. Septin 2 is often found associated with septin 7 or septin 9 in vertebrate systems. We found that septins 7 and 9 were expressed and localized
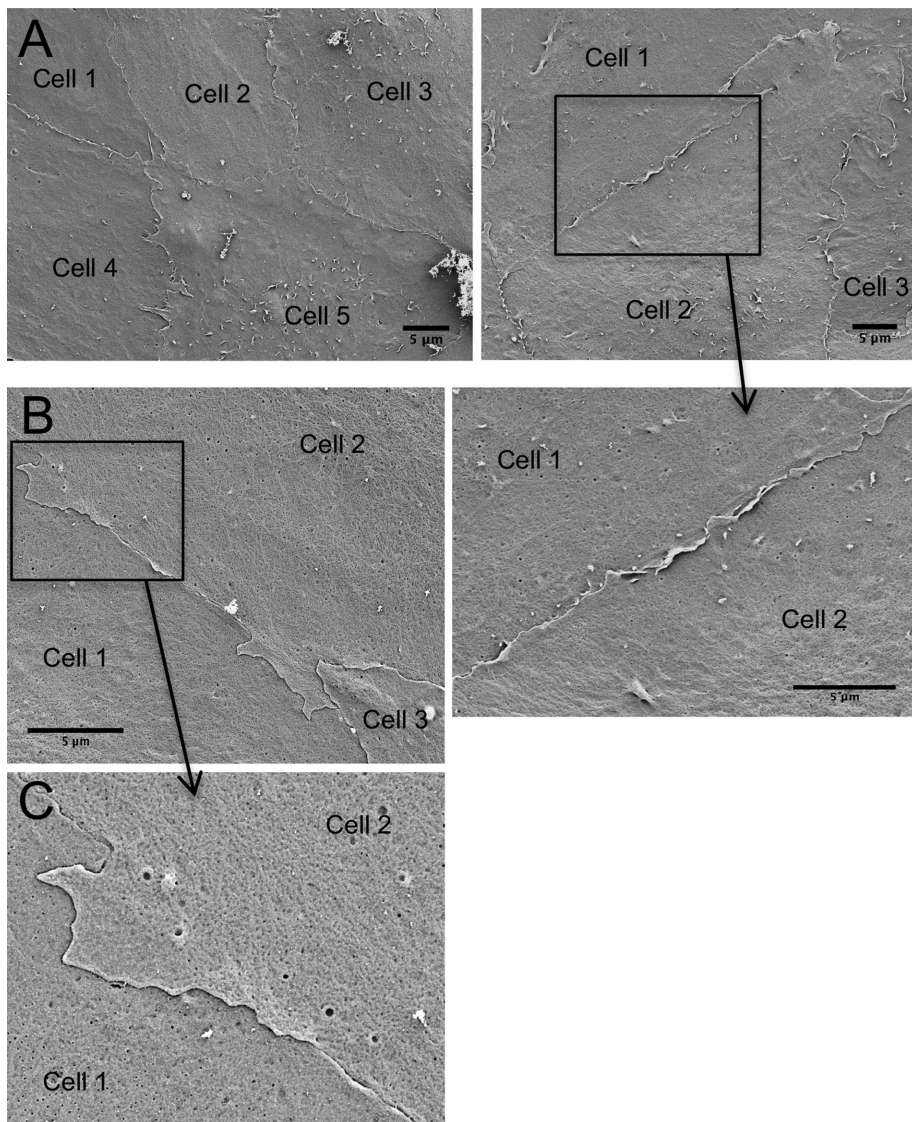
FIGURE 1: Surface views of cell junctions of human microvascular endothelial monolayers by scanning electron microscopy. (A) Low-magnification image of cell junctions between several cells. Scale bar, 5 μm. (B, C) Higher-magnification images of cell junctions. In many locations, the membranes at cell junctions are linear and smooth; in some cases, one cell protrudes over a neighbor. Some cell membranes show ruffles at the boundary. Scale bar = 5 μm.

also revealed that the levels of septin 7 and 9 depended on the level of septin 2 (Supplemental Figure 4B).

Quantitation of positive curvature

The amount of positive curvature displayed by septins associating with membranes has been measured in vitro with purified proteins and in vivo in fungal cells (Bridges *et al.*, 2016). Septins associating with lipid-coated beads showed a peak of association at a curvature of 2 μm^{-1}, with values extending from 0.31 to 6.67 μm^{-1}. We measured the radius of curved septin structure in our cells. The distribution was non-Gaussian, with a median of 2.2 μm^{-1} (Supplemental Figure 5). Values ranged from a minimum of 0.9 μm^{-1} to a maximum of 4.3 μm^{-1}, for 69 measurements from nine cells. Thus, these values for positive curvature in our cells are similar to those with purified components in vitro.

Localization of septin 2 and VE-cadherin in the *z*-axis

Septin 2 and VE-cadherin were both localized at cell junctions, but not in exactly the same locations. Septin 2 formed curved structures, while VE-cadherin formed straight linear structures. Both septin 2 and VE-cadherin are known to associate directly with plasma membranes. We hypothesized that the curved structures of septin 2 might be associated with protrusions of one cell above or below its neighbor, while VE-cadherin accumulated at more stable membrane-associated junctions, as illustrated in Figure 6A. Using structured illumination, we collected series of *x–y* planes of fluorescence staining of endogenous septin 2 and VE-cadherin from the bottom to the top of the specimen (Figure 6B). In some cases, septin 2 and VE-cadherin came into focus in different focal planes. Two examples are shown in Figure 6B, in the top and middle sets of panels of image. In these two cases, septin 2 appears in focus in early frames, near the bottom of the specimen, while VE-cadherin is in focus in later frames, near the top of the specimen. In these cases, one can envision that septin 2 is associated with membrane protrusions of one cell that lie underneath the neighboring cell. In other cases, especially where the specimen was thin, the *z*-axis resolution was not sufficient to distinguish septin 2 from VE-cadherin.

To understand the three-dimensional architecture of the cells in the endothelial monolayers, we examined thin sections of monolayers by transmission electron microscopy (Figure 7). Indeed, cells were quite thin, 100–200 nm in height. At cell–cell junctions, one cell was often on top of or below its neighboring cells. Some cases of ruffles were observed (Figure 7, A and B). In some cases, adjacent cells appeared to be pushing against one another (Figure 7C) and attempting to protrude above or below each other.

to cell junctions of HDMVEC monolayers, by immunofluorescence, in a distribution similar to that of septin 2 (Supplemental Figure 3). Septins 7 and 9 appeared in scallop-shaped and curved structures in association with the plasma membrane, as seen for septin 2, and those structures did not colocalize with VE-cadherin or F-actin. We did not observe expression of septins 6, 8, or 11 in our HDMVEC preparations, based on immunofluorescence. In other studies, septin 6 has been associated with septin 2 and septin 7; however, noncanonical sets of hetero-oligomers have been described (Valadares *et al.*, 2017). The negative result here with septin 6 may reflect a feature of human endothelial cells, or it may result from a technical issue, such as antibody reactivity.

Septins in complexes often depend on one other for stability. We found that suppression of septin 2 led to depletion of septins 7 and 9, based on immunofluorescence of cell junctions of endothelial monolayers (Supplemental Figure 4A). Immunoblot analysis
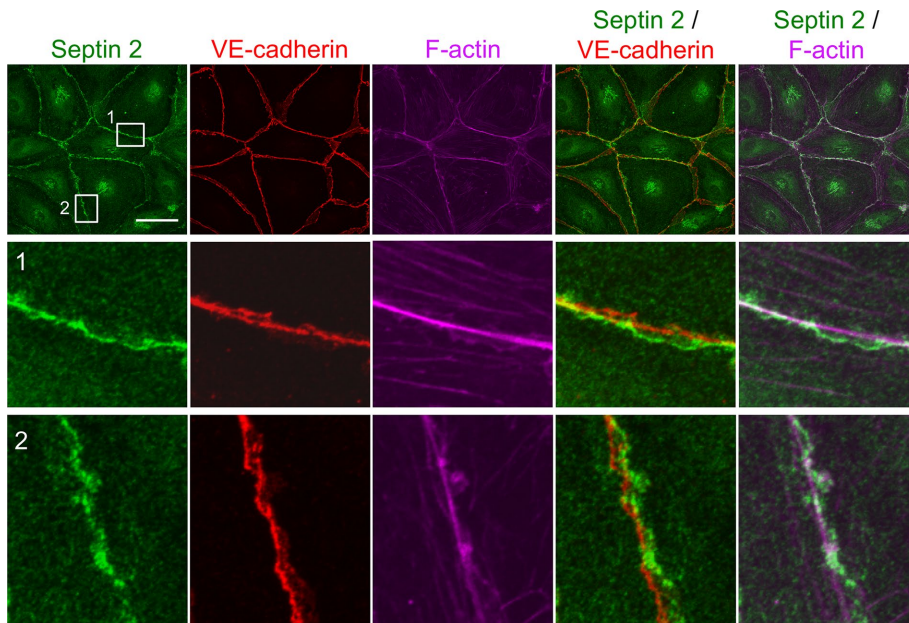
FIGURE 2: Localization of septin 2, VE-cadherin, and F-actin at cell junctions of endothelial monolayers. Immunofluorescence staining of endogenous septin 2 (green) and VE-cadherin (red), combined with fluorescent phalloidin staining for F-actin (magenta). Top row: scale bar = 50 µm. Middle and bottom rows are higher magnification images of the boxed regions 1 and 2, respectively. In these two-dimensional projections, septin 2, VE-cadherin and F-actin localize near each other at cell junctions but with distinct differences.
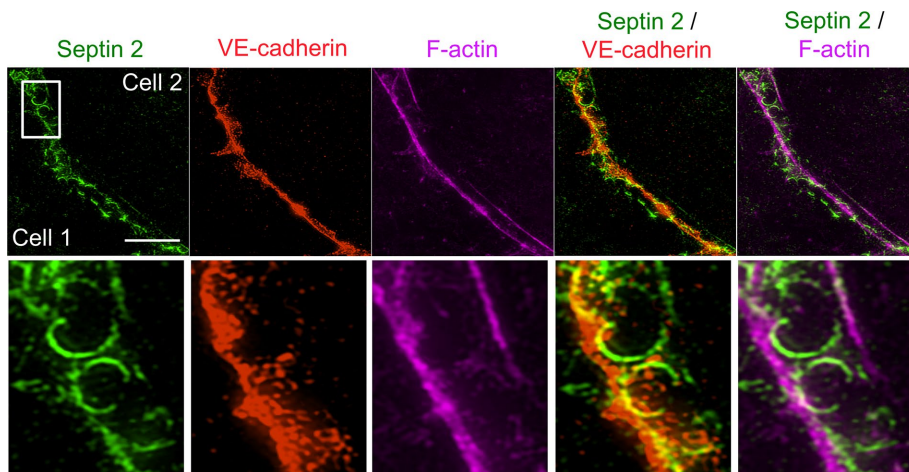

FIGURE 3: Scallop-shaped and curved structures of septin 2 at cell junctions of endothelial monolayers. Endogenous septin 2 (green), VE-cadherin (red), and F-actin (magenta) revealed by antibody and fluorescent phalloidin staining. Septin 2 appears in curved scallop shapes, resolved more clearly in higher magnification images of the boxed region. Images are two-dimensional projections of Z-stacks of scanning confocal image planes. Scale bar = 5 µm.

Functional role of septin 2 in endothelial monolayer integrity

To determine the functional roles of septin 2 in endothelial cell monolayers, we suppressed expression of septin 2 by infecting cells with lentiviruses carrying plasmids expressing short hairpin RNA (shRNA) targeting septin 2. Two shRNA oligonucleotides decreased the level of septin 2 by up to 96% (Figure 8A).

Septin 2–depleted cells showed alterations and discontinuities in the morphology of cell–cell junctions. By surface scanning electron microscopy (Supplemental Figure 6), septin 2–depleted monolayers showed gaps between cells (white asterisks) with spike-shaped

filopodial processes protruding above (black arrowheads) and underneath (white arrowheads) neighboring cells. The cells displayed an increased number of prominent linear fibers (black asterisks) in broad flattened cytoplasmic regions, consistent with an increase in F-actin stress fibers, which is described below.

Adherens and tight junctions are found between cells in endothelial monolayers. To assess adherens junctions in septin 2–depleted cells, we examined the distribution of VE-cadherin. In control cells, VE-cadherin appeared as a continuous and relatively thin line at boundaries between cells. Suppression of septin 2 led to alterations of VE-cadherin structure, resulting in these lines becoming broader, wavy, and discontinuous (Figure 8B and Supplemental Videos S1 and S2). In addition, suppression of septin 2 led to an increase in the staining intensity of VE-cadherin at cell junctions by immunofluorescence (Figure 8B) and increased total levels of VE-cadherin by immunoblot (Figure 8C).

Depletion of septin 2 also changed the arrangement of actin filaments. Control cells showed thick bundles of F-actin at cell junctions, underlying and in association with VE-cadherin. The interior of the cell contained thin actin fibers that were dispersed. On the other hand, septin 2–depleted cells showed decreased staining intensity of the bundles of F-actin at the cell junctions, along with increases in number and staining intensity of F-actin fibers passing through the cytoplasm (Figure 8B).

Tight junction molecules are also components contributing to junctional integrity, in association with F-actin. Therefore, we examined the tight junction protein ZO-1 at cell junctions in septin 2–depleted cells by immunofluorescence staining (Supplemental Figure 7). The pattern and distribution of ZO-1 showed some changes, not nearly as extensive as those for VE-cadherin. The ZO-1 staining intensity was decreased to a small to moderate extent in the septin 2–depleted cells, relative to control. Also, the linear junctional structures showed minor discontinuities that were less prominent than those observed for VE-cadherin.

Live-cell differential interference contrast imaging provided views of membrane protrusions and dynamic membrane remodeling in real time. Control cells showed occasional dynamic membrane ruffles at cell junctions, in association with intact and stable junctions (Supplemental Video S3). In contrast, septin 2–depleted cell membranes showed an increased prominence of retractions, resulting in gaps between cells, coupled with increased protrusions composed of broad and highly dynamic ruffles (Supplemental Video S4). The action of the ruffles appeared to contribute to closing these gaps.
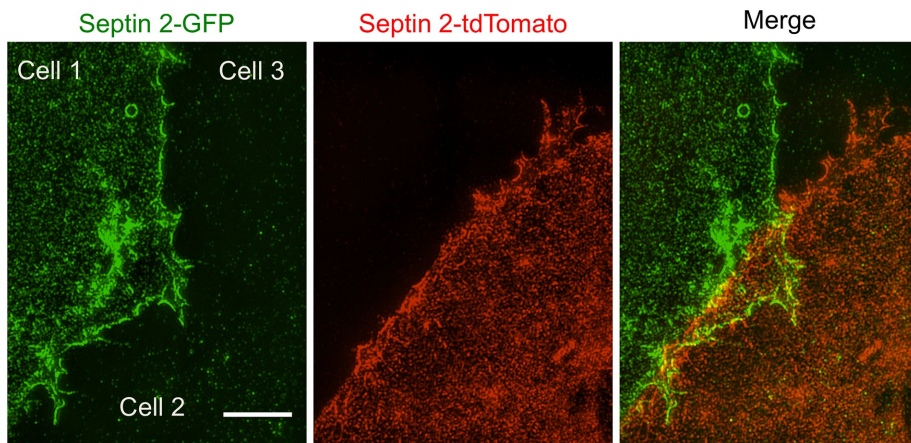
FIGURE 4: Septin 2 in curved structures at membranes with positive curvature. Cell junctions between three neighboring cells are shown. Cell 1 expresses septin 2-GFP, Cell 2 expresses septin 2-tdTomato, and Cell 3 expresses no fluorescent protein. The fluorescence patterns in Cells 2 and 3 reveal that septin 2 is present at regions of the cell edge with positive curvature. Two-dimensional projections of Z-stacks of scanning confocal images. Scale bar = 5 µm.
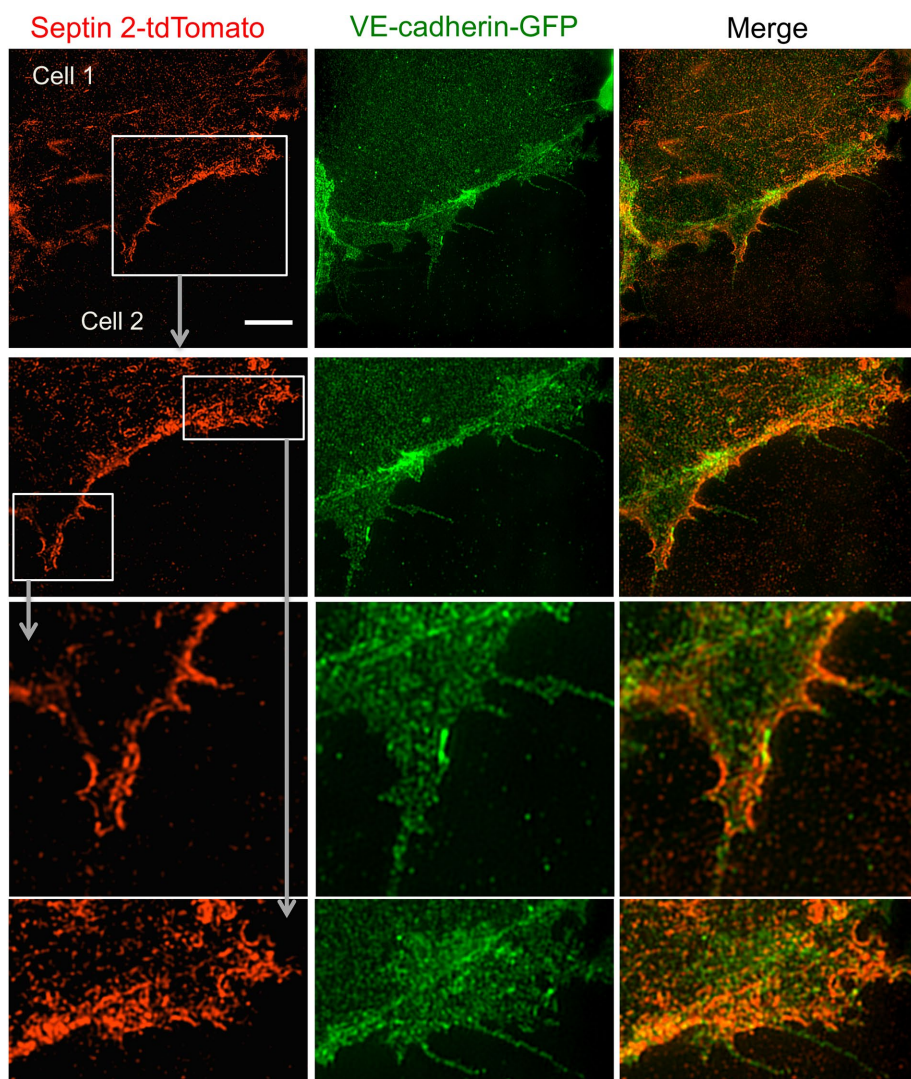

FIGURE 5: Septin 2 in curved structures at membranes with positive curvature. Cell 1 simultaneously expresses septin 2-tdTomato and VE-cadherin-GFP, adjacent to Cell 2, which does not express any fluorescent protein. VE-cadherin-GFP serves as a marker for the plasma

Barrier function of the endothelium

The endothelium is an important barrier between the circulation and tissues and cell–cell junctions are an important determinant of the strength of the barrier. VE-cadherin and actin filaments are known to play important roles in endothelial cell junction integrity (Mavrakis *et al.*, 2014; Mooren *et al.*, 2015). Accordingly, we asked whether septins are also important for the barrier function of the endothelium. The inflammatory mediator TNF-α activates endothelial cells, leading to a decrease in barrier integrity and a subsequent increase in transmigration of leukocytes. Therefore, we assessed the effects of the loss of septins on barrier integrity, and we compared those effects with the effect of TNF-α treatment.

First, we confirmed that TNF-α treatment of an endothelial monolayer, composed of HDMVECs, led to alterations in the arrangement and organization of VE-cadherin and F-actin (Figure 9A, rows 1 and 4). These effects of TNF-α were similar to those resulting from loss of septin 2 (Figure 9A, rows 2–4). TNF-α treatment also decreased the level of septin 2 accumulation at cell junctions, assessed by the fluorescence intensity of the stained preparations (Figure 9A, row 4). The level of septin 2 staining intensity in TNF-α–treated cells was similar to that observed with shRNA-induced depletion of septin 2. The combination of TNF-α treatment with suppression of septin 2 showed a small or no additive effect (Figure 9A). These results raise the possibility that the effects of TNF-α on VE-cadherin and F-actin at cell junctions were mediated by decreased levels of septin 2.

Next, we assessed monolayer barrier integrity by measuring transendothelial electrical resistance (TEER) across the monolayer. TEER values in septin 2–suppressed cell monolayers were decreased to values that were ~70% of those for control monolayers (Figure 9B). TEER values also decreased in TNF-α treated cells to a level of ~75% of control. In both cases, the differences were statistically significant with $p < 0.0001$. The combination of septin 2 suppression with TNF-α treatment led to a slightly further decrease in TEER values to ~50% of control. The smaller differences between the effects of single and double treatments (i.e.,

membrane. Distribution of septin 2-tdTomato shows that septin 2 is enriched at regions of positive curvature at the base and along the sides of membrane protrusions. The top panel is a low-magnification view. The bottom panels show higher-magnification views of the boxed regions. Scale bar = 5 µm.
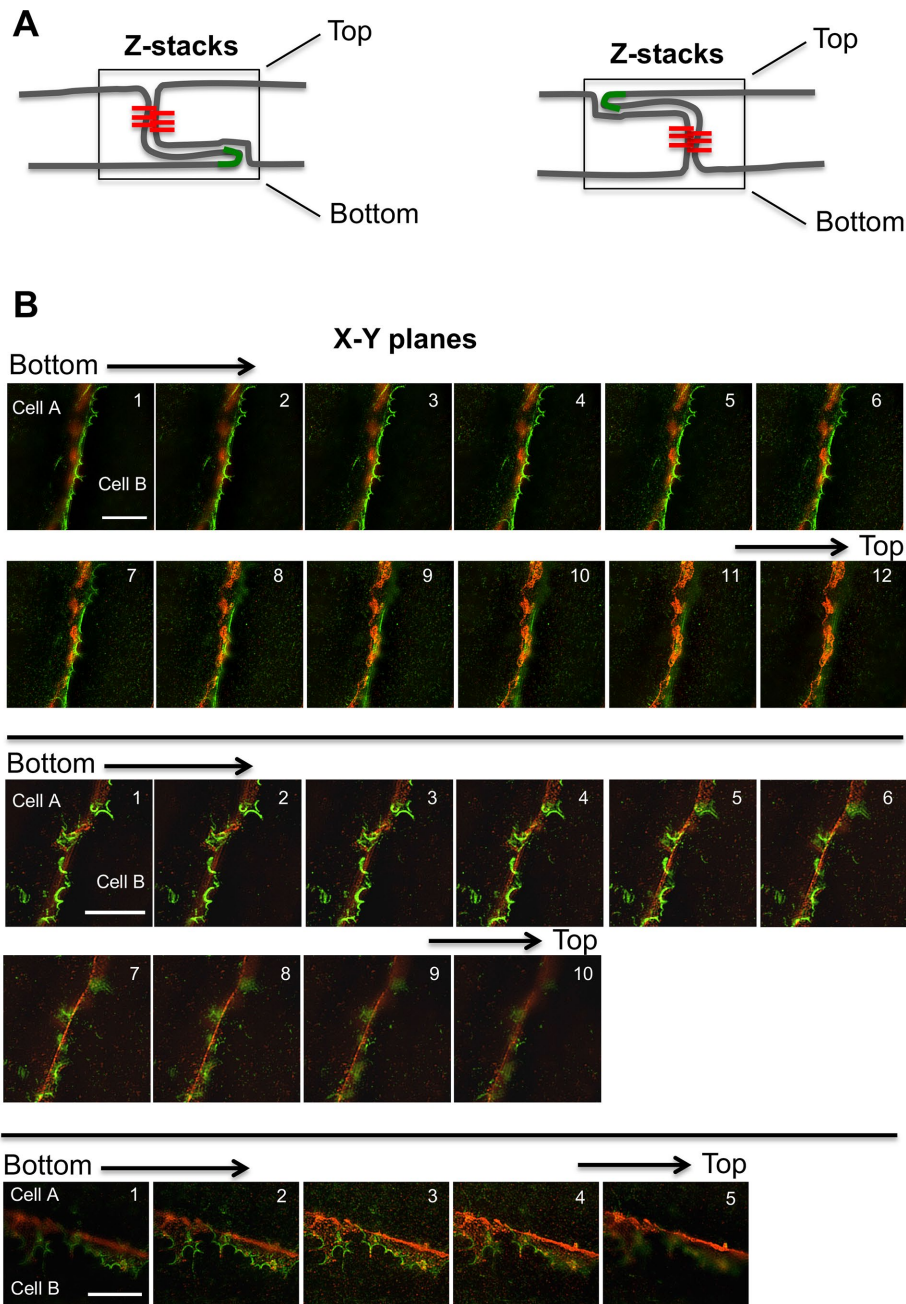
FIGURE 6: Localization of septin 2 and VE-cadherin at *z*-axis planes of cell junctions. (A) Diagrams illustrating possible *z*-axis locations for septin 2 (green) and VE-cadherin (red) at cell junctions. (B) *z*-Axis series of *x–y* focal planes of immunofluorescence staining for endogenous septin 2 (green) and VE-cadherin (red). In the first example, in the top two rows of images, septin 2 curved regions are in focus from frames 1 to 7 but fall out of focus from 8 to 12. In contrast, VE-cadherin appears in focus in frames 7 to 12. In the second example, septin 2 is in focus from frames 1 to 6, with VE-cadherin in focus from frames 4 to 9. In the third example, unlike the first two, septin 2 and VE-cadherin appear in focus in the same frames; this specimen is very thin, compared with the first two.

moving across the surface would stop moving and then migrate through and underneath the monolayer, where the NK cell would flatten between the monolayer and the substrate and then begin to migrate again. The change in morphology of the NK cells before and after transmigration facilitated scoring the events by direct visualization. The percentage of cells undergoing transendothelial migration (TEM) increased in septin 2–suppressed HMDVECs compared with control (Figure 9C). In independent experiments on different days with different primary cells, the baseline level of TEM for control cells differed; however, in each case, both of the two shRNAs targeting septin 2 consistently led to increases in the percentage of NK cells undergoing TEM. We suspect that the differences between experiments were most likely due to differences in the primary HDMVECs, which are derived from different sources and which change over time with passage in culture.

DISCUSSION

In this study, we discovered that septins are important for the proper assembly, dynamics, and stability of cadherin-based cell junctions between endothelial cells in a monolayer. Septins are also important for the integrity of the barrier function of the endothelial monolayer, based on their role in support of cell junctions.

Septin filament assembly and organization

Microvascular endothelial cell–cell contact sites are not static structures; the membranes and the adhesions constantly undergo dynamic remodeling. Local effects of septins on membrane protein composition, curvature, and rigidity can affect membrane shape and protrusive activity. Septin filaments are known to elongate at both ends and to bend at a certain length (median persistence, 12 μm) (Bridges *et al.*, 2014). Curved septin filaments associate with membranes of positive curvature, with curvature values ranging from 0.31 to 6.67 μm^{-1} (Bridges *et al.*, 2016). Here we found that endogenous septins were enriched at regions of cell–cell contact where the plasma membrane displayed positive curvature; the curvature values ranged from 1.0 to 4.2 μm^{-1}. We also observed septins in lesser amounts at regions of the plasma

TNF-α and septin 2 suppression) were also statistically significant, with $p < 0.001$. Thus, the effects of septin 2 depletion on TEER values mirrored the effects on VE-cadherin and F-actin distribution.

As an independent measure of endothelial barrier integrity, we assayed the transmigration of natural killer (NK) cells across the endothelial monolayers, based on direct visualization of living cells in time-lapse videos (Supplemental Videos S5–S7). A round NK cell

membrane without curvature. Together, our results are consistent with studies of septin association with membranes, both in vitro and in cells (Bridges *et al.*, 2014, 2016).

Assembly and dynamics of VE-cadherin–based cell junctions

We found that suppression of septin 2 dramatically altered the organization of VE-cadherin at cell–cell contact sites, and this was
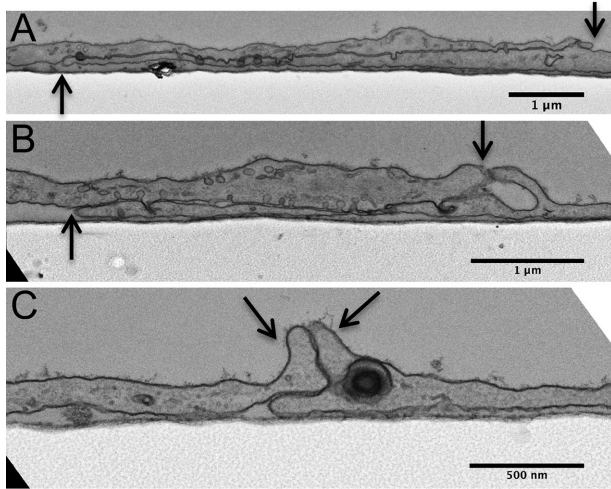
FIGURE 7: Transmission electron micrographs of sagittal thin sections of cell junctions of an endothelial monolayer. Thin membrane protrusions from neighboring cells extend toward each other cell and overlap to different extents. Scale bar = 1 µm for A and B and 500 nm for C.

FIGURE 8: Septin 2 suppression alters VE-cadherin arrangement at cell junctions and the level of VE-cadherin expression. (A) Decreased septin 2 expression in endothelial cells (HDMVECs) expressing shRNAs targeting septin 2. Immunoblot of whole-cell lysates probed with anti-septin 2 and anti-GAPDH as a control. Two different shRNA sequences targeting septin 2 decrease expression. (B) Immunofluorescence staining for endogenous septin 2, VE-cadherin, and F-actin. Control endothelial cells in the top panels, expressing a control shRNA, show intact junctional localization of septin 2, VE-cadherin, and F-actin. Cells expressing shRNA targeting septin 2, in the bottom panels, show decreased intensity of anti-septin 2 staining. The cells show altered VE-cadherin organization, with junction staining patterns that are broad, wavy, and discontinuous compared with control. F-actin imaging in these cells shows increased staining in the interior of the cell with less staining at cell junctions. Scale bar = 50 µm. (C) Increased VE-cadherin expression.

associated with a decrease in junctional integrity of human microvascular endothelial monolayers. Both septins and cadherin were enriched at sites of cell contact, but their localization patterns showed distinct differences. Superresolution light microscopy, with a careful examination of z-axis focal planes, was important to reveal these differences because the endothelial monolayer specimens were very thin. At cell contacts, septins could be observed below cadherin-based junctions, in cases where the contact region was sufficiently thick to permit z-axis resolution.

Actin-based lamellipodia are a prominent feature of endothelial cell junctions, and their assembly depends on Arp2/3 complex (Mooren *et al.*, 2014, 2015). Branched actin networks have been proposed to push membranes of adjacent cells toward each other to promote VE-cadherin interactions (Efimova and Svitkina, 2018). "Junction-associated intermittent lamellipodia" have been found to be important for cadherin-based cell junction formation during angiogenesis (Cao *et al.*, 2017). Here we found lamellipodial protrusions to be very thin and to extend above or below the neighboring cell; loss of septin 2 led to increased prominence of filopodial protrusions, gaps between cells and F-actin stress fibers in the cytoplasm, based on electron microscope images of surface and cross-section views.

In previous work on the role of cytoskeleton-associated proteins in VE-cadherin and junctional integrity, we found that two Arp2/3 complex nucleation-promoting factors, WAVE2 and N-WASp, regulated the junctional integrity of microvascular endothelial monolayers as measured by TEER (Mooren *et al.*, 2014, 2015). Surprisingly, the two Arp2/3 regulators had opposing effects. WAVE2 depletion decreased the level of VE-cadherin and disrupted the organization of VE-cadherin at cell–cell contacts, and this was accompanied by decreases in junctional integrity. In contrast, N-WASp depletion led to increased junctional integrity, coupled with a broadening of the cadherin-distribution at cell–cell contact sites but without a loss of cadherin accumulation. We proposed that the two Arp2/3 regulators played different roles; WAVE2 in promoting lamellipodial protrusions and early cell–cell contacts and N-WASp in promoting maturation or turnover of cellular junctions.

Interestingly, here we observed that the effects of septin 2 depletion on VE-cadherin at cell junctions and junctional integrity appears
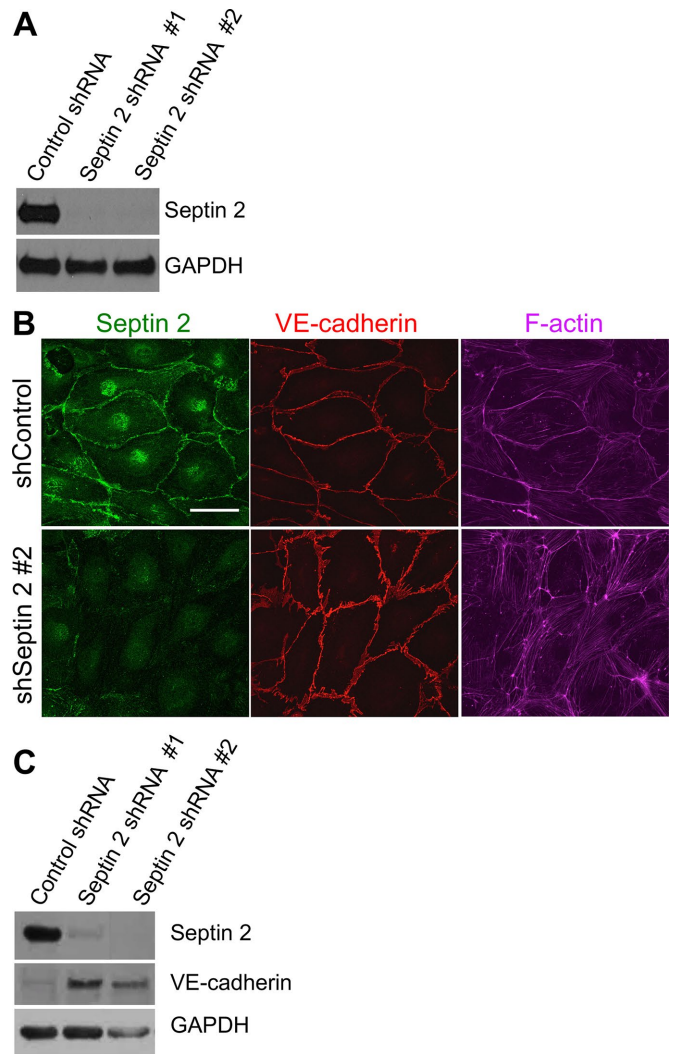
to be a combination of the phenotypes of WAVE2 and N-WASp depletion. Both WAVE2 and septin 2 depletion led to a decrease in barrier function and junctional integrity, as measured by TEER and loss of VE-cadherin expression. However, septin 2 depletion also led to a broader, discontinuous, and wavy distribution of VE-cadherin at cell junctions, similarly to what was observed for N-WASp depletion. We conclude that the cellular actions of septins are critical for the proper organization and level of VE-cadherin at endothelial cell junctions.
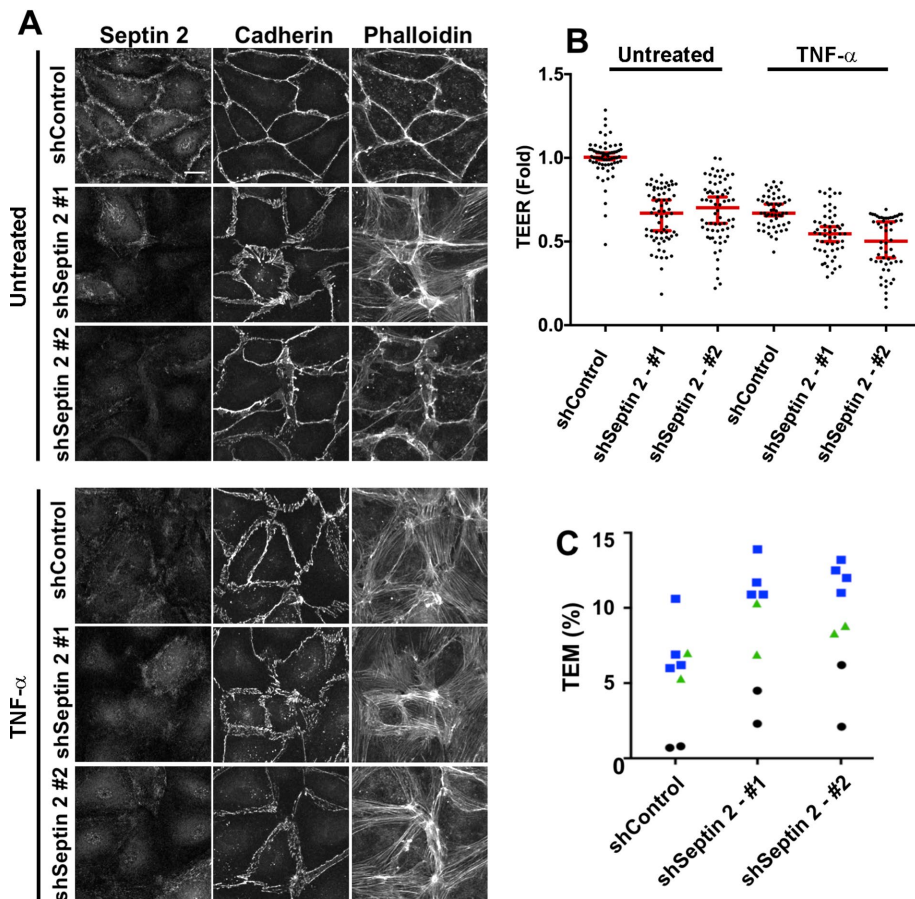
FIGURE 9: Decreased endothelial monolayer integrity in response to septin 2 depletion and TNF-α treatment. Endothelial cells (HDMVECs) expressing shRNAs targeting septin 2 and treated with TNF-α. (A) Immunofluorescence staining of endogenous septin 2 and VE-cadherin, with fluorescent phalloidin staining for F-actin of endothelial cell monolayers. Scale bar = 5 μm. Control cells, expressing shControl RNA, are shown in the top set of three panels, while the middle and bottom sets of panels show cells expressing two different shRNAs targeting septin 2. Cells were treated with TNF-α in the bottom set of panels and not the top set. TNF-α-treated cells show less septin 2 at cell junctions, with alterations of VE-cadherin and F-actin at cell junctions. These effects are similar to those caused by decreased septin 2. (B) Decreases in TEER in cells treated with TNF-α and with shRNAs targeting septin 2. Within each of 11–14 independent experiments, TEER values were normalized to 1 for shRNA control cells not treated with TNF-α. Treatment with TNF-α and shSeptin 2 knockdown decreased TEER values to ~70% of control. The combination of TNF-α with shSeptin 2 decreased the TEER values slightly further, to approximately 50–60% of control. The horizontal bar is the median of the values, and the error bars represent the 95% C.I. from the median. Statistical significance at a $p < 0.0001$ was found, by parametric t tests and nonparametric Mann–Whitney tests for all of the following pairwise comparisons: Untreated shControl vs. untreated shSeptin 2 #1 and #2; untreated shControl vs. treated shControl; and treated shControl vs. treated shSeptin2 #1 and #2. (C) Transendothelial migration by NK cells, scored as individual events from movies. Septin 2 shRNA expression led to increased levels of transendothelial migration compared with control. The results come from three independent experiments performed on different days, with each experiment as a different color: black, green, and blue. The absolute values differed among the three days, but the relative changes were similar. In each case, loss of septin 2 was associated with increased transendothelial migration.

Potential cellular mechanisms

The mechanism by which septin 2 regulates junctional integrity and VE-cadherin organization remains to be defined. On the basis of our results here and in previous studies, we speculate that septin-based assemblies act as support and stabilizers for F-actin–based protrusions that form by membrane-associated actin assembly. We found curved septin 2 structures predominantly in areas of protruding

plasma membrane. Septins have been observed in association with filopodial and lamellopodial protrusions, the formation and retraction of which depend on actin assembly and disassembly (Kinoshita *et al.*, 2002; Spiliotis and Nelson, 2008; Hu *et al.*, 2012; Nölke *et al.*, 2016). Septins at regions of positive curvature at the base of protrusions may promote the extension of the protrusion by providing structural support, and they may inhibit or limit the progression of retraction of protrusions by acting as a structural barrier.

Septins have been found to play interactive roles with actin and microtubule networks as part of the regulation of cellular processes in other settings (Kinoshita *et al.*, 2002; Hu *et al.*, 2008, 2012; Nölke *et al.*, 2016). Here we observed control HDMVECs to have thick actin filament bundles at cell junctions; septin 2 depletion led to a thinning of these bundles with increased appearance of thin F-actin bundles in the form of a loose network dispersed about the cytoplasm. These results are consistent with a coordinated action of septin and F-actin in the processes of local membrane remodeling.

Summary and conclusions

Endothelial cells have septins associated with their plasma membrane, and septins accumulate at regions of positive curvature in association with cell junctions. Septins are important for cadherin-based cell junctions, and therefore for the integrity of the barrier function of the endothelial monolayer. Septin arrays may function as mechanical support for actin-based protrusions, which are known to be important for the assembly and stability of cadherin-based cell junctions.

MATERIALS AND METHODS
Cells and cell culture

Primary HDMVECs from neonates were obtained from Lonza (Walkersville, MD) and cultured in Microvascular Endothelial Cell Growth Medium-2 (EGM-2MV) medium from Lonza (Walkersville, MD). Primary HBMVECs were obtained from ScienCell Research Laboratories (San Diego, CA) and cultured in endothelial cell medium from ScienCell Research Laboratories (San Diego, CA). For experiments, these primary cells were used between passages 3 and 8.

Natural killer-92 (NK-92) cells were obtained from the American Type Culture Collection (Manassas, VA) and cultured in alpha-MEM with 12.5% horse serum and 12.5% fetal bovine serum (FBS), 2 mM L-glutamine and 1.5 g/l sodium bicarbonate, 0.2 mM inositol, 0.1 mM 2-mercaptoethanol, 0.02 mM folic acid supplemented with 10 U/ml Interleukin-2 (IL-2). HEK293T cells were grown in DMEM containing 10% FBS and 1% streptomycin/penicillin.

Antibodies and reagents

A monoclonal mouse anti-human VE-cadherin antibody (clone 55-7H1) was obtained from BD Biosciences (San Jose, CA), and polyclonal rabbit anti-human septin 2, 7, and 9 antibodies were obtained from Sigma Life Science Prestige Antibodies (St. Louis, MO). A monoclonal mouse anti-ZO-1 antibody (clone ZO-1 1A12) was obtained from Invitrogen (Rockford, IL). A monoclonal mouse anti-human GAPDH (clone 6C5), used as an internal loading control, was obtained from Abcam (Cambridge, MA). Anti-GFP mouse monoclonal antibody (9F9.F9) and anti-RFP rabbit polyclonal antibody preadsorbed were obtained from Rockland Immunochemicals (Limerick, PA). Secondary antibodies and phalloidin conjugated with fluorescent Alexa dyes and secondary antibodies conjugated with horseradish peroxidase were obtained from Molecular Probes ThermoFisher (Eugene, OR) and Sigma-Aldrich (St. Louis, MO), respectively.

Tumor necrosis factor alpha (TNF-α) was obtained from Life Technologies ThermoFisher (Gaithersburg, MD), and fibronectin was obtained from Sigma-Aldrich. Interleukin-2 was obtained from GenScript (Piscataway, NJ). Prolong Gold anti-fade solution was obtained from Molecular Probes ThermoFisher. SuperScript III First-Strand Synthesis System for reverse transcription-PCR (RT–PCR) and T4 DNA Ligase were obtained from Invitrogen Life Technologies (Carlsbad, CA). PfuTurbo DNA polymerase was obtained from Agilent Technologies (Santa Clara, CA).

Nucleic acid reagents

Two shRNA oligonucleotides targeting septin 2 and one shRNA oligonucleotide targeting LacZ, to serve as a control, were obtained from the McDonnell Genome Institute at Washington University in St. Louis. The septin 2 shRNA oligonucleotides were GCCCTTAGATGTGGCGTTTAT (508-528, oligo #1, pBJ2457) and CCCAGGACCTTCATTATGAAA (872-892, oligo #2, pBJ2458). The LacZ shRNA oligonucleotide was CGCGCCTTTCGGCGGTGAAAT. shRNAs targeting septin 7 (TRCN0000322631, oligo #1, pBJ2460, and TRCN0000146634, oligo #2, pBJ2461) and septin 9 (TRCN0000119068, pBJ2462) from the MISSION shRNA collection were obtained from Sigma Aldrich.

To create a lentiviral plasmid expressing human septin 2, total RNA was isolated from HDMVECs and cDNA was synthesized using SuperScript III First-Strand Synthesis System for RT–PCR (Life Technologies). The septin 2 coding region was PCR amplified with primers containing AgeI and XbaI restriction sites. The amplified PCR product was subcloned into the pBOB-GFP (pBJ2464, gift of George Bloom, University of Virginia, Charlottesville, VA) and pBOB-tdTomato (pBJ2465) lentiviral plasmids.

To create a lentiviral plasmid expressing fluorescent human VE-cadherin, we obtained mApple-VE-cadherin-N10 from Addgene (cat. no. 54959, Cambridge, MA). The VE-cadherin coding region was PCR amplified with primers containing AgeI and XbaI restriction sites, and the PCR product was subcloned into the pBOB-GFP lentiviral plasmid (Marr et al., 2004).

Lentivirus production and infection

Lentiviruses were produced using a third-generation system with conditional packaging (Dull et al., 1998). Briefly, HEK293T cells were grown in 150-mm dishes and transfected with two packing plasmids, pRRE (10.9 μg, Gag and Pol) and pRSV-REV (4.12 μg, Rev), an envelope plasmid pMD2.G (6 μg, VSV-G), and a transfer plasmid including shRNA or cDNA (7.5 μg). After 1 d, culture medium was replaced with DMEM containing 30% FBS. After 2 more days, the medium containing lentiviruses was collected, filtered with 0.45-μm-pore–sized membranes (EMD Millipore, Billerica,

MA) and concentrated by ultracentrifugation at 20,000 rpm at 4°C for 2 h.

HDMVECs grown in six-well plates were incubated with lentivirus carrying shRNA-expressing plasmids targeting septin genes in culture medium with 1 μg/ml protamine sulfate for 1 d and then placed into fresh medium. For live-cell imaging and immunofluorescence staining, cells were transferred to 14-mm glass-bottom dishes (Mat-Tek Corp., Ashland, MA) and cultured for an additional 3 d. Ectopic expression of fluorescent VE-cadherin was performed with the same method. To suppress septin 2 expression and express fluorescent VE-cadherin, cells were first incubated with lentivirus carrying shRNA plasmids targeting septin 2 in a six-well plate for 1 d and then transferred to glass-bottom dishes. After the cells settled down, they were incubated with lentivirus carrying plasmids expressing fluorescent VE-cadherin cDNA for 1 d in medium containing 1 μg/ml protamine sulfate. Cells were placed into fresh medium and cultured for another 3 d.

Immunofluorescence staining

Confluent HDMVEC monolayers were fixed by adding an equal volume of 2X fixation solution (5% paraformaldehyde in PIPES [piperazine-N,N′-bis(2-ethanesulfonic acid)] buffer, prewarmed to 37°C) (Mooren et al., 2009) directly into culture dishes and incubated at 37°C for 10 min. Next, cell samples were permeabilized by incubation with 0.1% Triton X-100 in phosphate-buffered saline (PBS) for 5 min at room temperature (RT). Samples were incubated in blocking buffer (3% bovine serum albumin [BSA] in PBS) for at least 30 min, in primary antibodies diluted in blocking buffer overnight at 4°C, and in secondary antibodies conjugated with Alexa fluorescent dyes diluted in blocking buffer for 1 h at RT. Cells were washed with PBS three times after primary and secondary antibody incubations. For phalloidin staining, fluorescent phalloidin was added to the secondary antibody dilution mixture. Samples were mounted with ProLong Gold anti-fade reagent.

Fluorescence imaging was performed with a Nikon A1R resonant scanning confocal system and a Nikon N-SIM structured illumination superresolution microscope system. With the A1R, a 60× objective was used, Z-stacks were collected with a 0.188 μm step size, and images are presented as two-dimensional projections of Z-stacks. With the SIM, a 100× objective was used, Z-stacks were collected with 0.1 or 0.2 μm steps, and images are presented as two-dimensional projections of Z-stacks or as single focal planes.

Electron microscopy

We performed scanning electron microscopy (SEM) of whole-culture specimens to visualize the surface of the endothelial monolayer of control and septin 2–depleted HDMVECs. HDMVECs infected with lentivirus were cultured on glass coverslips coated with 15 μg/ml fibronectin until cells reached confluency and formed a monolayer. Cells were briefly rinsed in 0.1 M cacodylate buffer prewarmed to 37°C and then fixed with 2.5% glutaraldehyde and 2% paraformaldehyde in 0.1 M cacodylate buffer with 2 mM CaCl₂, pH 7.4, at 37°C. The coverslips were incubated at 37°C for 5 min and then moved to RT for 1 h. Coverslips were rinsed in 0.1 M cacodylate buffer three times for 5 min each, followed by secondary fixation in 1% OsO₄ in 0.1 M cacodylate buffer for 30 min in the dark. Coverslips were rinsed three times in ultrapure water for 5 min each followed by 2% aqueous tannic acid for 30 min. After another three water washes, the samples were stained in 2% aqueous uranyl acetate for 30 min, briefly water-washed, and then dehydrated in a graded ethanol series (30%, 40%, 50%, 60%, 70%, 80%, 90%, 100% ×2), with 5 min at each step. Once dehydrated, coverslips were loaded into a critical

point drier (Leica EM CPD 300, Vienna, Austria) set to perform 12 CO_2 exchanges at the slowest speed. The dried coverslips were mounted on aluminum stubs with carbon adhesive tabs and sputter-coated with 6 nm of iridium (Leica ACE 600, Vienna, Austria). After coating, the samples were loaded into a FE-SEM (Zeiss Merlin, Oberkochen, Germany) and imaged at 3 keV with a probe current of 300 pA using the Everhart Thornley secondary electron detector.

To visualize cross-sections of cells and cell junctions, we performed transmission electron microscopy of thin sections of plastic-embedded samples. HDMVECs were cultured on plastic (ACLAR) coverslips coated with 15 µg/ml fibronectin, fixed with aldehydes as described above for SEM, rinsed in 0.1 M cacodylate buffer three times for 5 min each and secondarily fixed in 1% OsO_4 with 1.5% potassium ferrocyanide in 0.1 M cacodylate buffer for 1 h in the dark. Coverslips were rinsed three times in ultrapure water for 5 min each, then stained en bloc with 2% aqueous uranyl acetate for 1 h. After a brief water wash, samples were dehydrated in a graded acetone series (50%, 70%, 90%, 100% ×2) with 10 min at each step and then infiltrated into LX112 resin with microwave assistance. Coverslips were then flat embedded between two ACLAR coverslips and polymerized at 60°C for 48 h. The ACLAR coverslips were peeled away from the resin, and small areas were excised and mounted perpendicularly on a blank epoxy stub for cross-sectioning. Sections of 70 nm were cut and imaged on a transmission electron microscope (JEOL JEM-1400 Plus, Tokyo, Japan) at 80 keV.

Live-cell imaging
At 4 d postinfection, confluent HDMVECs were used for live-cell imaging. To view membrane protrusions and VE-cadherin dynamics, time-lapse images were collected on a Nikon A1R laser scanning confocal microscope using a 20× objective. Time-lapse images were collected every 20 s for 1 h, with control of temperature at 37°C and CO_2 at 5% in a stage incubator (Tokai Hit, Fujinomiya, Japan).

Immunoblots
Confluent HDMVECs were washed with RT PBS and lysed by adding ice-cold 1% NP-40 lysis buffer into culture dishes and incubating on ice for at least 30 min. Cell lysates were harvested by scraping the dish, and they were centrifuged at 13,000 rpm for 15 min at 4°C. The supernatant was incubated with SDS-loading buffer, boiled for 5 min, electrophoresed on SDS–PAGE gels, and transferred to polyvinylidene difluoride membrane (EMD Millipore Corp.) at 90 V for 1 h. The membrane was incubated in blocking buffer (4% BSA in TBST buffer) and then in a primary antibody mixture overnight at 4°C. After washing with PBS, the membrane was incubated in horseradish-peroxidase–conjugated secondary antibodies at RT for 1 h. The membrane was incubated with enhanced chemiluminescence solution for 5 min at RT and developed for autoradiography.

Transendothelial electric resistance
At 2 d postinfection with lentivirus carrying plasmids expressing septin 2 or control shRNA, HDMVECs were transferred into fibronectin-coated 24 transwell inserts (3×10^4 cells/insert) and grown to form confluent monolayers for approximately 2–3 d. For experiments with TNF-α treatment, cells placed into culture medium with 20 ng/ml TNF-α and incubated overnight; untreated cells were placed into culture medium without TNF-α.

Transendothelial electric resistance (TEER) was measured using an Endohm-6 electrode adapter with an EVOM-2 m (World Precision Instruments, Sarasota, FL). TEER values were calculated by subtracting the resistance values for empty transwell inserts (no endo-thelial cells) from resistance values for transwell inserts with endothelial cells and then multiplying those values by the surface area of the transwell. The values for experimental samples were calculated as fold changes compared with the average of control samples. Statistical significance was calculated with GraphPad Prism, using parametric unpaired t tests and nonparametric Mann–Whitney tests.

Transendothelial cell migration assay
At 2 d post–lentivirus infection, HDMVECs were transferred into 14-mm glass-bottom culture dishes (MatTek Corporation, Ashland, MA). After 2–3 d in culture, when the cells achieved confluency, 5 µl of an NK cell suspension (5×10^5 cells/ml) was dropped onto a monolayer. After the NK cells settled down onto the surface of the HDMVEC monolayer, live-cell images were collected using an inverted microscope (Olympus IX-81) with a 10× NA objective, a Hg-lamp light source and a Hamamatsu electron-multiplying charge-coupled device video camera at 20-s intervals for 1 h. Videos were analyzed using ImageJ, transmigration events were counted, and TEM percentage was calculated as the number of transmigrated NK cells divided by the total number of NK cells added.

REFERENCES
Abbott NJ, Rönnbäck L, Hansson E (2006). Astrocyte-endothelial interactions at the blood-brain barrier. Nat Rev Neurosci 7, 41–53.

Abu Taha A, Taha M, Seebach J, Schnittler HJ (2014). ARP2/3-mediated junction-associated lamellipodia control VE-cadherin-based cell junction dynamics and maintain monolayer integrity. Mol Biol Cell 25, 245–256.

Baldwin AL, Thurston G (2001). Mechanics of endothelial cell architecture and vascular permeability. Crit Rev Biomed Eng 29, 247–278.

Bazzoni G, Dejana E (2004). Endothelial cell-to-cell junctions: molecular organization and role in vascular homeostasis. Physiol Rev 84, 869–901.

Bertin A, McMurray MA, Pierson J, Thai L, McDonald KL, Zehr EA, García G, Peters P, Thorner J, Nogales E (2012). Three-dimensional ultrastructure of the septin filament network in Saccharomyces cerevisiae. Mol Biol Cell 23, 423–432.

Bezanilla M, Gladfelter AS, Kovar DR, Lee WL (2015). Cytoskeletal dynamics: a view from the membrane. J Cell Biol 209, 329–337.

Bridges AA, Gladfelter AS (2015). Septin form and function at the cell cortex. J Biol Chem 290, 17173–17180.

Bridges AA, Jentzsch MS, Oakes PW, Occhipinti P, Gladfelter AS (2016). Micron-scale plasma membrane curvature is recognized by the septin cytoskeleton. J Cell Biol 213, 23–32.

Bridges AA, Zhang H, Mehta SB, Occhipinti P, Tani T, Gladfelter AS (2014). Septin assemblies form by diffusion-driven annealing on membranes. Proc Natl Acad Sci USA 111, 2146–2151.

Cao J, Ehling M, März S, Seebach J, Tarbashevich K, Sixta T, Pitulescu ME, Werner AC, Flach B, Montanez E, et al. (2017). Polarized actin and VE-cadherin dynamics regulate junctional remodelling and cell migration during sprouting angiogenesis. Nat Commun 8, 2210.

Deanfield JE, Halcox JP, Rabelink TJ (2007). Endothelial function and dysfunction: testing and clinical relevance. Circulation 115, 1285–1295.

Dejana E (2004). Endothelial cell-cell junctions: happy together. Nat Rev Mol Cell Biol 5, 261–270.

Dolat L, Hu Q, Spiliotis ET (2014). Septin functions in organ system physiology and pathology. Biol Chem 395, 123–141.

Dolat L, Spiliotis ET (2016). Septins promote macropinosome maturation and traffic to the lysosome by facilitating membrane fusion. J Cell Biol 214, 517–527.

Dull T, Zufferey R, Kelly M, Mandel RJ, Nguyen M, Trono D, Naldini L (1998). A third-generation lentivirus vector with a conditional packaging system. J Virol 72, 8463–8471.

Efimova N, Svitkina TM (2018). Branched actin networks push against each other at adherens junctions to maintain cell-cell adhesion. J Cell Biol 217, 1827–1845.

Finnigan GC, Duvalyan A, Liao EN, Sargsyan A, Thorner J (2016). Detection of protein-protein interactions at the septin collar in *Saccharomyces cerevisiae* using a tripartite split-GFP system. Mol Biol Cell 27, 2708–2725.

Fung KY, Dai L, Trimble WS (2014). Cell and molecular biology of septins. Int Rev Cell Mol Biol 310, 289–339.

Garcia-Ponce A, Citalán-Madrid AF, Velázquez-Avila M, Vargas-Robles H, Schnoor M (2015). The role of actin-binding proteins in the control of endothelial barrier integrity. Thromb Haemost 113, 20–36.

Haarer BK, Pringle JR (1987). Immunofluorescence localization of the *Saccharomyces cerevisiae CDC12* gene product to the vicinity of the 10-nm filaments in the mother-bud neck. Mol Cell Biol 7, 3678–3687.

Hartsock A, Nelson WJ (2008). Adherens and tight junctions: structure, function and connections to the actin cytoskeleton. Biochim Biophys Acta 1778, 660–669.

Hu J, Bai X, Bowen JR, Dolat L, Korobova F, Yu W, Baas PW, Svitkina T, Gallo G, Spiliotis ET (2012). Septin-driven coordination of actin and microtubule remodeling regulates the collateral branching of axons. Curr Biol 22, 1109–1115.

Hu Q, Nelson WJ, Spiliotis ET (2008). Forchlorfenuron alters mammalian septin assembly, organization, and dynamics. J Biol Chem 283, 29563–29571.

Joo E, Surka MC, Trimble WS (2007). Mammalian SEPT2 is required for scaffolding nonmuscle myosin II and its kinases. Dev Cell 13, 677–690.

Kang H, Lew DJ (2017). How do cells know what shape they are? Curr Genet 63, 75–77.

Kinoshita M, Field CM, Coughlin ML, Straight AF, Mitchison TJ (2002). Self- and actin-templated assembly of Mammalian septins. Dev Cell 3, 791–802.

Lalor PF, Lai WK, Curbishley SM, Shetty S, Adams DH (2006). Human hepatic sinusoidal endothelial cells can be distinguished by expression of phenotypic markers related to their specialised functions in vivo. World J Gastroenterol 12, 5429–5439.

Lampugnani MG, Dejana E, Giampietro C (2017). Vascular endothelial (VE)-cadherin, endothelial adherens junctions, and vascular disease. Cold Spring Harb Perspect Biol 2017, a029322.

Marr RA, Guan H, Rockenstein E, Kindy M, Gage FH, Verma I, Masliah E, Hersh LB (2004). Neprilysin regulates amyloid Beta peptide levels. J Mol Neurosci 22, 5–11.

Mavrakis M, Azou-Gros Y, Tsai FC, Alvarado J, Bertin A, Iv F, Kress A, Brasselet S, Koenderink GH, Lecuit T (2014). Septins promote F-actin ring formation by crosslinking actin filaments into curved bundles. Nat Cell Biol 16, 322–334.

Michiels C (2003). Endothelial cell functions. J Cell Physiol 196, 430–443.

Mooren OL, Kim J, Li J, Cooper JA (2015). Role of N-WASP in endothelial monolayer formation and integrity. J Biol Chem 290, 18796–18805.

Mooren OL, Kotova TI, Moore AJ, Schafer DA (2009). Dynamin2 GTPase and cortactin remodel actin filaments. J Biol Chem 284, 23995–24005.

Mooren OL, Li J, Nawas J, Cooper JA (2014). Endothelial cells use dynamic actin to facilitate lymphocyte transendothelial migration and maintain the monolayer barrier. Mol Biol Cell 25, 4115–4129.

Nölke T, Schwan C, Lehmann F, Østevold K, Pertz O, Aktories K (2016). Septins guide microtubule protrusions induced by actin-depolymerizing toxins like Clostridium difficile transferase (CDT). Proc Natl Acad Sci USA 113, 7870–7875.

Ong K, Wloka C, Okada S, Svitkina T, Bi E (2014). Architecture and dynamic remodelling of the septin cytoskeleton during the cell cycle. Nat Commun 5, 5698.

Pachter JS, de Vries HE, Fabry Z (2003). The blood-brain barrier and its role in immune privilege in the central nervous system. J Neuropathol Exp Neurol 62, 593–604.

Pagliuso A, Tham TN, Stevens JK, Lagache T, Persson R, Salles A, Olivo-Marin JC, Oddos S, Spang A, Cossart P, Stavru F (2016). A role for septin 2 in Drp1-mediated mitochondrial fission. EMBO Rep 17, 858–873.

Poisson J, Lemoinne S, Boulanger C, Durand F, Moreau R, Valla D, Rautou PE (2017). Liver sinusoidal endothelial cells: physiology and role in liver diseases. J Hepatol 66, 212–227.

Rodal AA, Kozubowski L, Goode BL, Drubin DG, Hartwig JH (2005). Actin and septin ultrastructures at the budding yeast cell cortex. Mol Biol Cell 16, 372–384.

Schnittler H, Taha M, Schnittler MO, Taha AA, Lindemann N, Seebach J (2014). Actin filament dynamics and endothelial cell junctions: the ying and yang between stabilization and motion. Cell Tissue Res 355, 529–543.

Spiliotis ET, W J Nelson (2008). Septin Functions in the Mammalian Cytoskeleton, Hoboken, NJ: John Wiley & Sons, Ltd, 229–246.

Spiliotis ET (2018). Spatial effects-site-specific regulation of actin and microtubule organization by septin GTPases. J Cell Sci 131, jcs207555.

Spiliotis ET, Gladfelter AS (2012). Spatial guidance of cell asymmetry: septin GTPases show the way. Traffic 13, 195–203.

Spiliotis ET, Hunt SJ, Hu Q, Kinoshita M, Nelson WJ (2008). Epithelial polarity requires septin coupling of vesicle transport to polyglutamylated microtubules. J Cell Biol 180, 295–303.

Spiliotis ET, Nelson WJ (2006). Here come the septins: novel polymers that coordinate intracellular functions and organization. J Cell Sci 119, 4–10.

Sumpio BE, Riley JT, Dardik A (2002). Cells in focus: endothelial cell. Int J Biochem Cell Biol 34, 1508–1512.

Valadares NF, d' Muniz Pereira H, Ulian Araujo AP, Garratt RC (2017). Septin structure and filament assembly. Biophys Rev 9, 481–500.